Draft Modified August 9, 2016
Preprint typeset using LaTeX style emulateapj v. 12/16/11

EFFECT OF SURFACE-MANTLE WATER EXCHANGE PARAMETERIZATIONS ON EXOPLANET OCEAN DEPTHS

Thaddeus D. Komacek[1] & Dorian S. Abbot[2]
[1]Lunar and Planetary Laboratory, Department of Planetary Sciences, University of Arizona
[2]Department of the Geophysical Sciences, University of Chicago
Draft Modified August 9, 2016

ABSTRACT

Terrestrial exoplanets in the canonical habitable zone may have a variety of initial water fractions due to random volatile delivery by planetesimals. If the total planetary water complement is high, the entire surface may be covered in water, forming a "waterworld." The habitable zone for waterworlds is likely smaller than that for planets with partial land coverage because waterworlds lack the stabilizing continental silicate-weathering feedback. On a planet with active tectonics, competing mechanisms act to regulate the abundance of water on the surface by determining the partitioning of water between interior and surface. Here we explore how the incorporation of different mechanisms for the degassing and regassing of water changes the volatile evolution of a planet. We explore three models for volatile cycling: a model with degassing and regassing both determined by the seafloor pressure, one with mantle temperature-dependent degassing and regassing rates, and a hybrid model that has the degassing rate driven by seafloor pressure and the regassing rate determined by the mantle temperature. We find that the volatile cycling in all three of these scenarios reaches a steady-state after ~ 2 Gyr. Using these steady-states, we find that if volatile cycling is either solely temperature-dependent or pressure-dependent, exoplanets require a high abundance ($\gtrsim 0.3\%$ of total mass) of water to have fully inundated surfaces. This is because the waterworld boundary for these models is regulated by how much water can be stuffed into the mantle. However, if degassing is more dependent on seafloor pressure and regassing mainly dependent on mantle temperature, the degassing rate is relatively large at late times and a steady-state between degassing and regassing is reached with a substantial surface water fraction. If this hybrid model is physical, super-Earths with a total water fraction similar to that of the Earth ($\sim 0.06\%$ by mass) can become waterworlds. As a result, further understanding of the processes that drive volatile cycling on terrestrial planets is needed to determine the water fraction at which they are likely to become waterworlds.

Subject headings: methods: analytical – planets and satellites: terrestrial planets – planets and satellites: interiors – planets and satellites: oceans – planets and satellites: tectonics

1. INTRODUCTION

1.1. *Surface water abundance and habitability*

To date, the suite of observed exoplanets from *Kepler* has proven that Earth-sized planets are common in the universe (≈ 0.16 per star, Fressin et al. 2013; Morton & Swift 2014). Though we do not yet have a detailed understanding of the atmospheric composition of an extrasolar terrestrial planet, spectra of many extrasolar gas giants (Kreidberg et al. 2015; Sing et al. 2015) and a smaller Neptune-sized planet (Fraine et al. 2014) have shown that water is likely abundant in other Solar Systems. Calculations of volatile delivery rates to terrestrial planets via planetesimals (e.g. Raymond et al. 2004) have shown that planets can have a wide range of initial water fractions, with some planets being 1% water by mass or more. Both observations and simulations hence point towards the likelihood that terrestrial planets are also born with abundant water. However, the intertwined effects of climate (Kasting et al. 1993) and mantle-surface volatile interchange (Hirschmann 2006; Cowan 2015) determine whether there is abundant liquid water on the present-day surfaces of terrestrial exoplanets. Additionally, atmospheric escape (especially early in the atmospheric evolution) can cause loss of copious amounts of water (Ramirez & Kaltenegger 2014; Luger & Barnes 2015; Tian & Ida 2015; Schaefer et al. 2016), with $\gtrsim 10$ Earth oceans possibly lost from planets in the habitable zone of M-dwarfs.

The extent of the traditional habitable zone is determined by the continental silicate weathering thermostat (Kasting 1988), in which silicate minerals react with CO_2 and rainwater to produce carbonates (Walker et al. 1981). Silicate weathering is extremely efficient at stabilizing the climate because the process runs faster with increasing temperature. This is due to faster reaction rates and increased rain in warmer climates. However, the silicate weathering thermostat itself depends on the surface water abundance.

If there is no surface water, the silicate weathering thermostat cannot operate due to the lack of reactants, and if the planet surface is completely water-covered the negative feedback does not operate unless seafloor weathering is also temperature dependent (Abbot et al. 2012). Note that even if seafloor weathering is temperature-dependent, it might be insufficient to stabilize the climate (Foley 2015). A waterworld state is likely stable (Wordsworth & Pierrehumbert 2013), as water loss rates would be low because the atmosphere would be CO_2-rich due to the lack of a silicate-weathering feedback. However, if water loss rates remain high due to a large incident stellar flux, it is possible that brief exposures

of land can allow for a "waterworld self-arrest" process in which the planet adjusts out of the moist greenhouse state (Abbot et al. 2012). This can occur if the timescale for CO_2 drawdown by the silicate-weathering feedback is shorter than the timescale for water loss to space, which is probable for Earth parameters. To determine whether or not waterworlds should be common, we must look to the deep-water cycle, that is, the mantle-surface interchange of water over geologic time.

1.2. *Earth's deep-water cycle*

To understand the deep-water cycle on exoplanets, we look to Earth as an analogue, as it is the only planet known with continuous (not episodic) mantle-surface water interchange due to plate tectonics. On present-day Earth, water is largely expelled from the mantle (degassed) through volcanism at mid-ocean ridges and volcanic arcs (Hirschmann 2006). Water is lost to the mantle (regassed) through subduction of hydrated basalt. The relative strength of regassing and degassing determines whether the surface water abundance increases or decreases with time.

It has long been suggested that Earth's surface water fraction is in effective steady-state (McGovern & Schubert 1989; Kasting & Holm 1992), due to the constancy of continental freeboard since the Archean (~ 2.5 Gya). However, this may simply be due to isostasy, that is, the adjustment of the continental freeboard under varying surface loads (Rowley 2013; Cowan & Abbot 2014). Additionally, the degassing and regassing rates on Earth are high enough that if they did not nearly balance each other the surface would have long ago become either completely dry or water-covered (Cowan & Abbot 2014). However, some studies of volatile cycling on Earth that utilized parameterized convection to determine the upper mantle temperature and hence the degassing and regassing rates have not found such a steady state (McGovern & Schubert 1989; Crowley et al. 2011; Sandu et al. 2011). If the Earth is indeed near steady-state, this mismatch could be because there are many secondary processes, e.g. loss of water into the transition zone (Pearson et al. 2014) and early mantle degassing (Elkins-Tanton 2011), that are difficult to incorporate into a simplified volatile cycling model. Alternatively, Earth's mantle evolution may not have progressed far enough to reach an effective steady-state. Lastly, it is possible that our understanding of what processes control the release of water from the mantle and return of water to it via subduction is incomplete.

Using the maximum allowed fraction of water in mantle minerals (Hauri et al. 2006; Inoue et al. 2010), Cowan & Abbot (2014) estimate that Earth's mantle water capacity is ≈ 12 times the current surface water mass. However, measurements of the electrical conductivity of Earth's mantle (Dai & Karato 2009) have found only $\sim 1-2$ ocean masses of water in the mantle, which is much less than the maximally allowed value. This measurement may vary spatially (Huang et al. 2005) and by method (Khan & Shankland 2012), but it is likely constrained to within a factor of a few. This implies that dynamic effects lead to a first-order balance between degassing and regassing on Earth, rather than the surface water complement being in steady-state simply because the mantle is saturated.

1.3. *Previous work: the deep-water cycle on super-Earths*

Using a steady-state model wherein the degassing and regassing of water is regulated by seafloor pressure, Cowan & Abbot (2014) applied our knowledge of Earth's deep-water cycle to terrestrial exoplanets. They showed that terrestrial exoplanets require large amounts ($\sim 0.1\%$ by mass) of delivered water to become waterworlds. Applying a time-dependent model and including the effects of mantle convection, Schaefer & Sasselov (2015) found that the amount of surface water is strongly dependent on the details of the convection parameterization. These works rely on other planets being in a plate-tectonic regime similar to Earth. However, it is important to note that there is debate about whether or not plate tectonics is a typical outcome of planetary evolution (e.g. O'Neill & Lenardic 2007; Valencia et al. 2007a; Valencia & O'Connell 2009; Korenaga 2010), potentially because plate tectonics is a history-dependent phenomenon (Lenardic & Crowley 2012). In this work, we also assume plate tectonics. We do so because our understanding of habitability is most informed by Earth and it enables us to examine how processes that are known to occur on Earth affect water cycling on exoplanets. In the future, exploring other tectonic regimes (e.g. stagnant lid) may be of interest to exoplanet studies and potential investigations of Earth's future evolution (Sleep 2015).

The studies of volatile cycling on super-Earths discussed above used drastically different approaches, with Cowan & Abbot (2014) applying a two-box steady-state model of volatile cycling, and Schaefer & Sasselov (2015) extending the time-dependent coupled volatile cycling-mantle convection model of Sandu et al. (2011) to exoplanets. As a result, these works made different assumptions about which processes control water partitioning between ocean and mantle. The degassing parameterization of Cowan & Abbot (2014), based on the model of Kite et al. (2009), utilized the negative feedback between surface water inventory and volatile degassing rate that results from pressure reducing degassing. Their regassing rate was also related to the surface water inventory, using the prediction of Kasting & Holm (1992) that the hydration depth increases with increasing surface water abundance up to the limit where the hydration depth is equal to the crustal thickness. Meanwhile, the degassing and regassing parameterizations of Schaefer & Sasselov (2015) were both related directly to the mantle temperature, with the degassing rate determined by the abundance of water in melt and the regassing rate set by the depth of the hydrated basalt (serpentinized) layer, which is determined by the depth at which the temperature reaches the serpentinization temperature.

In this work, we seek to identify how different assumptions about regassing and degassing determine the surface water mass fraction. To do so, we utilize simplified models of convection and volatile cycling that separately incorporate the key features of both the Cowan & Abbot (2014) and Schaefer & Sasselov (2015) volatile cycling parameterizations. The latter model builds upon the analytic work of Crowley et al. (2011), who developed an analytic model that captures the key processes in the numerical models of Sandu et al. (2011) and Schaefer & Sasselov (2015). However, here we fur-

ther simplify and also non-dimensionalize the Crowley et al. (2011) model, enabling us to elucidate the dependencies of water abundance on mantle temperature and planetary parameters. We then combine the models of Cowan & Abbot (2014) and Schaefer & Sasselov (2015), utilizing surface water budget-dependent degassing and temperature-dependent regassing. We do so because it is likely the most physically relevant choice, as temperature affects serpentinization depths (and resulting regassing rates) more directly than seafloor pressure. Additionally, temperature-dependent degassing would become small at late times seafloor pressure-dependent degassing does not, and it has been shown by Kite et al. (2009) that degassing should be pressure-dependent. This is more in line with the approximate steady-state water cycling on Earth is currently in, as if both regassing and degassing are temperature-dependent regassing will dominate at late times. We find that the choice of volatile cycling parameterization greatly impacts the end-state surface water mass reservoir. We also find that, regardless of volatile cycling parameterization, the water partitioning reaches a steady-state after a few billion years of evolution due to the cooling of the mantle to below the melting temperature, which causes the effective end of temperature-dependent degassing and regassing.

This paper is organized as follows. In Section 2, we describe our parameterized convection model and the various volatile cycling parameterizations we explore, along with the consequences these have for the temporal evolution of mantle temperature and water mass fraction. Detailed derivations of the volatile cycling models can be found in Appendix A. In Section 4 we explore where in water mass fraction-planet mass parameter space each volatile cycling model predicts the waterworld boundary to lie. We discuss our results in Section 5, performing a sensitivity analysis of the waterworld boundary on key controlling parameters, comparing this work to previous works, and discussing our limitations and potential avenues for future work. Importantly, we also show how our model with pressure-dependent degassing and temperature-dependent regassing could in principle be observationally distinguished from the models of Cowan & Abbot (2014) and Schaefer & Sasselov (2015). Lastly, we express conclusions in Section 6.

2. COUPLING MANTLE CONVECTION AND VOLATILE CYCLING

2.1. *Parameterized convection*

Parameterized convection models utilize scalings from numerical calculations to relate the Nusselt number (the ratio of outgoing heat flux from the mantle to that which would be conducted if the entire mantle were not convecting) to the global mantle Rayleigh number (Turcotte & Schubert 2002). We here consider a standard boundary-layer convection model, as in McGovern & Schubert (1989) and Sandu et al. (2011), with top and bottom boundary layers of equal thickness and one characteristic mantle temperature. Figure 1 shows a schematic of the temperature profile relevant for this convection parameterization. This scaling takes the power-law form

$$\frac{F}{F_{\rm cond}} \equiv \mathrm{Nu} = a\left(\frac{\mathrm{Ra}}{\mathrm{Ra}_{\rm crit}}\right)^{\beta}, \tag{1}$$

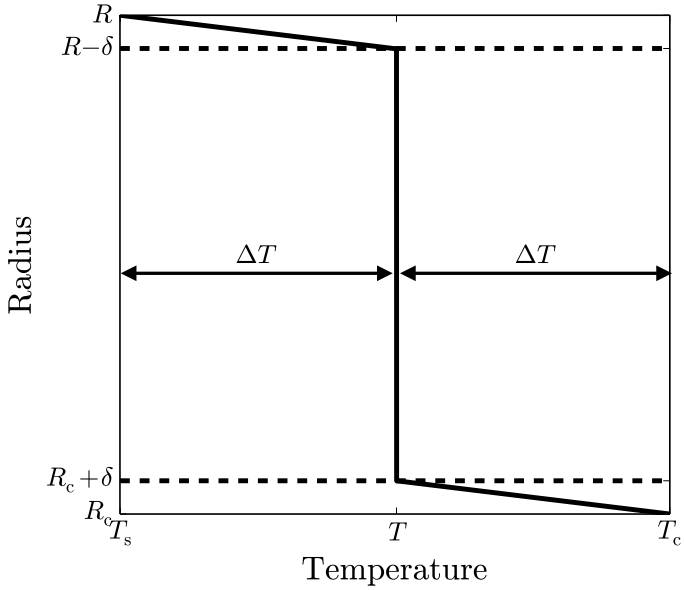

FIG. 1.— Schematic of the temperature profile utilized for the parameterized convection model. The mantle temperature, T is constant with depth throughout the convecting mantle. Conducting boundary layers form at the top and bottom (above and below the dashed lines) of this convecting interior, assumed to be of equal thickness δ. Given that these boundary layers have equal thicknesses, they must have equal temperature contrasts ΔT across them. Here R is planet radius, $R_{\rm c}$ is core radius, $T_{\rm s}$ is surface temperature, and $T_{\rm c}$ is the core temperature. Note that we do not consider the core heat evolution in this work, but have included it here to show the symmetry between the top and bottom boundary layers in this model.

where Nu is the Nusselt number, F is the convected flux, $F_{\rm cond} = k\Delta T/h$ is the flux that would be conducted if the mantle were not convecting, with k thermal conductivity, $h(M)$ is mantle thickness (which is a function of planetary mass M, see Section 2.1.1 for details), $\mathrm{Ra}_{\rm crit}$ is the critical Rayleigh number above which convection occurs, $\Delta T = T - T_{\rm s}$ is the temperature difference between mantle and surface, and $\beta \approx 0.3$. As in Schaefer & Sasselov (2015) we set $a = 1$, as a is an order-unity parameter. The global Rayleigh number is defined as

$$\mathrm{Ra} = \frac{\alpha\rho_{\rm m} g(M)\Delta T h^3(M)}{\eta(x,T)\kappa}, \tag{2}$$

where κ is the thermal diffusivity and α the thermal expansivity of the boundary layer, $\rho_{\rm m}$ the density of the mantle, $g(M)$ gravity, and $\eta(x,T)$ the mantle viscosity (which is a function of mantle water mass fraction, x, and temperature). The viscosity parameterization will be discussed further in Section 2.1.2.

Given the flux conducted out of the mantle from Equation (1), we can write down a thermal evolution equation that allows us to solve for the mantle temperature as a function of time and mantle water mass fraction. This is

$$\rho_{\rm m} c_p \frac{dT}{dt} = Q - \frac{A(M)F(T,x)}{V(M)}, \tag{3}$$

where c_p is the mantle heat capacity, $Q = Q_0 e^{-t/\tau_{\rm decay}}$ is the heating rate from radionuclides with $\tau_{\rm decay} = 2$ Gyr[1],

[1] we do not include the Kelvin-Helmholtz contraction term which is small at late times

$A(M)$ is the planet surface area, and $V(M)$ is the mantle volume. We will non-dimensionalize Equation (3) in Section 2.1.3 to elucidate its dependence on temperature and mantle water mass fraction.

2.1.1. *Scaling with planet mass*

To calculate mass-dependent planetary parameters (h, A, V, g) we use the scaling laws of Valencia et al. (2006) that take into account internal compression effects on the radius. These scaling relations utilize a constant core mass fraction to relate the planetary radius R and core radius R_c to planetary mass

$$\begin{aligned} R &= R_\oplus \left(\frac{M}{M_\oplus}\right)^{p}, \\ R_\mathrm{c} &= cR_\oplus \left(\frac{M}{M_\oplus}\right)^{p_\mathrm{c}}, \end{aligned} \tag{4}$$

where $p = 0.27$, $c = 0.547$, $p_\mathrm{c} = 0.25$. Using Equation (4), we can then calculate $h = R - R_\mathrm{c}$, $A = 4\pi R^2$, $V = 4\pi/3(R^3 - R_\mathrm{c}^3)$, $g = GM/R^2$.

2.1.2. *Viscosity*

The mantle viscosity depends both on temperature and mantle water fraction. As noted by McGovern & Schubert (1989), this leads to a feedback in which increasing mantle water fraction decreases temperature, keeping mantle viscosity approximately constant. We use a similar parameterization as Sandu et al. (2011) and Schaefer & Sasselov (2015) for the mantle viscosity, however, we choose not to incorporate the pressure-dependence of viscosity. We do so because we are interested in convection driven by upper boundary peel-off, which occurs in the upper mantle where pressures are relatively small. This can be thought of as exploring the upper limit to the outgoing heat flux from the mantle, since assigning the viscosity in the middle or deep mantle would cause a decreased rate of planetary heat loss. We show in Section 3.1 that this choice of viscosity approximates Earth's mantle temperature well when we choose Earth-like parameters parameters. Our viscosity is hence parameterized as

$$\eta \approx \eta_0 f_\mathrm{w}^{-r} \exp\left[\frac{E_\mathrm{a}}{R_\mathrm{gas}}\left(\frac{1}{T} - \frac{1}{T_\mathrm{ref}}\right)\right], \tag{5}$$

where η_0 gives the viscosity scale, E_a is activation energy, R_gas is the universal gas constant, T_ref is the mantle melting temperature, and f_w is the water fugacity. We assume throughout this work that $r = 1$, which is the nominal value used by Schaefer & Sasselov (2015) and that expected from experiments on wet diffusion in olivine (Hirth & Kohlstedt 2003). As in Schaefer & Sasselov (2015), we relate the water abundance to fugacity using experimental data on the concentrations of water in olivine from Li et al. (2008) as

$$\begin{aligned} \ln f_\mathrm{w} = c_0 &+ c_1 \ln\left(\frac{Bx\mu_\mathrm{oliv}/\mu_\mathrm{w}}{1 - x\mu_\mathrm{oliv}/\mu_\mathrm{w}}\right) \\ &+ c_2 \ln^2\left(\frac{Bx\mu_\mathrm{oliv}/\mu_\mathrm{w}}{1 - x\mu_\mathrm{oliv}/\mu_\mathrm{w}}\right) + c_3 \ln^3\left(\frac{Bx\mu_\mathrm{oliv}/\mu_\mathrm{w}}{1 - x\mu_\mathrm{oliv}/\mu_\mathrm{w}}\right), \end{aligned} \tag{6}$$

where $c_0 = -7.9859$, $c_1 = 4.3559$, $c_2 = -0.5742$, $c_3 = 0.0227$, $B = 2 \times 10^6$ is a conversion to number concentration (H atom/10^6 Si atoms), μ_oliv is the molecular weight of olivine and μ_w is the molecular weight of water. As in Schaefer & Sasselov (2015), we choose η_0 such that $\eta(x = x_\oplus, T = T_\mathrm{ref}) = 10^{21}$Pa s which yields mantle temperatures that approximately reproduce those on Earth.

2.1.3. *Non-dimensional thermal evolution equation*

Throughout the remainder of this paper, we will work with non-dimensional versions of the thermal evolution and volatile cycling equations. We do so because it elucidates the essential physical processes and controlling non-dimensional variables. Substituting our scaling for mantle heat flux from Equation (1) into Equation (3) and using our prescription for viscosity from Equation (5), we can non-dimensionalize the thermal evolution equation as

$$\begin{aligned} \frac{d\tilde{T}}{d\tau_\mathrm{heat}} = \tilde{Q}(\tau_\mathrm{heat}) \\ - \tilde{F}_0 \tilde{f}_\mathrm{w}^{\beta}(\tilde{x}) \left(\tilde{T} - \tilde{T}_\mathrm{s}\right)^{\beta+1} \exp\left[-\frac{\beta}{\tilde{T}_\mathrm{m}}\left(\frac{1}{\tilde{T}} - 1\right)\right], \end{aligned} \tag{7}$$

where the non-dimensional temperature is $\tilde{T} = T/T_\mathrm{ref}$, the non-dimensional mantle water mass fraction is $\tilde{x} = x f_\mathrm{m}/(\omega_0 \tilde{f}_\mathrm{b})$, and $\tilde{F}_0 = F_0/Q_0$, where Q_0 is a constant and

$$F_0 = \frac{k T_\mathrm{ref}^{1+\beta} A}{hV}\left(\frac{\alpha \rho_\mathrm{m} g h^3 f_\mathrm{w}(\tilde{x}=1)}{\mathrm{Ra}_\mathrm{crit}\kappa\eta_0}\right)^{\beta}, \tag{8}$$

where the non-dimensional fugacity is $\tilde{f}_\mathrm{w} = f_\mathrm{w}/f_\mathrm{w}(\tilde{x} = 1)$, the melting temperature is $\tilde{T}_\mathrm{m} = T_\mathrm{ref} R_\mathrm{gas}/E_\mathrm{a}$, and the surface temperature is $\tilde{T}_\mathrm{s} = T_\mathrm{s}/T_\mathrm{ref}$. Lastly, the non-dimensional heating timescale is $\tau_\mathrm{heat} = tQ_0/(\rho_\mathrm{m} c_p T_m)$. The typical values of these non-dimensional parameters are shown in Table 1.

2.2. *Volatile cycling*

We seek to explore a variety of different volatile cycling parameterizations, each of which relies on the following expression for the time rate of change of mantle water mass fraction (Cowan & Abbot 2014)

$$\frac{dx}{dt} = \frac{L_\mathrm{MOR} S(T)}{f_\mathrm{m} M}\left(w_\downarrow - w_\uparrow\right), \tag{9}$$

where $S(T)$ is the temperature-dependent spreading rate (discussed further in Section 2.2.2), $f_\mathrm{m}M$ the mantle mass (where f_m is the mantle mass fraction), $w_\downarrow$ the regassing rate and $w_\uparrow$ the degassing rate. Each of the volatile cycling parameterizations we consider utilizes different regassing and degassing rates, which we explore in the following Sections 2.2.1-2.2.3.

2.2.1. *Seafloor pressure-dependent degassing and regassing*

In this section, we construct a non-dimensional version of Equation (9) corresponding to the volatile cycling model of Cowan & Abbot (2014). This model determines the water mass fraction of the mantle independent of the

Quantity	Symbol	Fiducial value
Mantle water mass fraction*	$\tilde{x}$	$\tilde{x}_\oplus = 1.32$
Mantle temperature*	$\tilde{T}$	$\tilde{T}_{\rm ref} = 1$
Planet mass	$\tilde{M}$	1
Total water mass fraction	$\tilde{\omega}$	2.07
Heating timescale	$\tau_{\rm heat}$	$t(\tau_{\rm heat} = 1) = 4.02$ Gyr
Pressure-dependent volatile cycling timescale	τ	$t(\tau = 1) = 2.87$ Gyr
Temperature-dependent volatile cycling timescale	$\tau_{\rm SS}$	$t(\tau_{\rm SS} = 1) = 2.22$ Gyr
Hybrid volatile cycling timescale	$\tau_{\rm hyb}$	$t(\tau_{\rm hyb} = 1) = 2.22$ Gyr
Heat flux	$\tilde{F}_0$	0.531
Heat flux scaling coefficient	β	0.3
Critical Rayleigh number	$\mathrm{Ra}_{\rm crit}$	1100
Water fugacity	$\tilde{f}_{\rm w}$	1
Surface temperature	$\tilde{T}_{\rm s}$	0.175
Reference temperature	$\tilde{T}_{\rm m}$	0.040
Mantle water mass fraction of Earth	$\tilde{X}_\oplus$	1.32
Seafloor pressure degassing exponent	μ	1
Seafloor pressure regassing exponent	σ	1
Solidus temperature	$\tilde{T}_{\rm sol,dry}$	0.780
Liquidus temperature	$\tilde{T}_{\rm liq,dry}$	0.936
Temperature-dependent degassing coefficient	Π	0.102
Solidus depression constant	$\tilde{\lambda}$	8.16×10^{-5}
Solidus depression coefficient	γ	0.75
Melt fraction exponent	θ	1.5
Pressure-dependent degassing coefficient	$\tilde{E}$	0.473
Maximum mantle water mass fraction	$\tilde{x}_{\rm max}$	15.9

TABLE 1
Non-dimensional variables and parameters used in this paper, their symbols, and and their value for Earth-like parameters. Stars denote model variables.

mantle temperature. We utilize their expressions for the regassing and degassing rates:

$$w_\downarrow = x_{\rm h}\rho_{\rm c} d_{\rm h}(P)\chi, \tag{10}$$

$$w_\uparrow = x\rho_{\rm m} d_{\rm melt} f_{\rm degas}(P), \tag{11}$$

where $x_{\rm h}$ is the mass fraction of water in the hydrated crust, $\rho_{\rm c}$ is the density of the oceanic crust, χ is the subduction efficiency, $\rho_{\rm m}$ is the density of the upper mantle, and $d_{\rm melt}$ is the depth of melting below mid-ocean ridges. As in Cowan & Abbot (2014), we take the depth of the serpentinized layer $d_{\rm h}(P)$ and the fraction of the water in the melt that is degassed $f_{\rm degas}(P)$ to be power-laws with seafloor pressure, with $d_{\rm h}$ increasing with increasing pressure and $f_{\rm degas}$ decreasing with increasing pressure. See Appendix A.1 for a thorough explanation of these parameters and the derivation that follows to give the mantle water mass fraction rate of change with time. Inserting Equations (10) and (11) into Equation (9) and non-dimensionalizing, we find

$$\frac{d\tilde{x}}{d\tau} = \left[\tilde{g}^2\left(\tilde{\omega} - \tilde{x}\right)\right]^\sigma - \tilde{X}_\oplus^{-1}\tilde{x}\left[\tilde{g}^2\left(\tilde{\omega} - \tilde{x}\right)\right]^{-\mu}. \tag{12}$$

In Equation (12),

$$\tilde{X}_\oplus = \frac{x_h\rho_{\rm c}\chi d_{\rm h,\oplus} f_{\rm M}}{\rho_{\rm m} d_{\rm melt} f_{\rm degas,\oplus}\omega_0 \tilde{f}_{\rm b}} \tag{13}$$

is a degassing coefficient identified by Cowan & Abbot (2014) as the mantle water mass fraction of Earth, $\tilde{\omega} = \omega/(\omega_0\tilde{f}_{\rm b})$ is the normalized total water mass fraction, $\tilde{g} = g/g_\oplus$, and

$$\tau_{\rm CA} = \tau = t\frac{L_{\rm MOR} S x_{\rm h}\rho_{\rm c}\chi d_{\rm h,\oplus}}{M\omega_0\tilde{f}_{\rm b}} \tag{14}$$

is the non-dimensional time, which is inversely related to the seafloor overturning timescale $A/(L_{\rm MOR}S)$. In this model, the spreading rate S and mid-ocean ridge length $L_{\rm MOR}$ are constants, but they will not be in Sections 2.2.2 and 2.2.3. We write the non-dimensional timescale here as τ because it will be the timescale that all of our solutions are converted to for inter-comparison.

2.2.2. *Temperature-dependent degassing and regassing*

In this section, we write down a simplified, non-dimensional form of Section 2.3 in Schaefer & Sasselov (2015). Their degassing and regassing rates are

$$w_\downarrow = x_{\rm h}\rho_{\rm c}\chi d_{\rm h}(T), \tag{15}$$

$$w_\uparrow = \rho_{\rm m} d_{\rm melt} f_{\rm degas,\oplus} f_{\rm melt}(T) x. \tag{16}$$

Equation (15) is identical to Equation (10) except now the hydrated layer depth is a function of temperature (see Appendix A.2 for details), and Equation (16) is similar to Equation (11) except $f_{\rm degas}(P)$ has been replaced by $f_{\rm degas,\oplus} f_{\rm melt}(T)$ with $f_{\rm melt}(T)$ the temperature-dependent mass fraction. In Equation (16) we have assumed that the mass fraction of water in melt is the same as the mass fraction of water in the mantle due to the extremely low ($\approx 1\%$) difference in water partitioning between melt and mantle rock.

Inserting our expressions (15) and (16) for regassing and degassing rates into Equation (9) and non-dimensionalizing, we find (see Appendix A.2 for the steps

and parameterizations of $S(T), d_{\rm h}(T), f_{\rm melt}(T)$)

$$\begin{aligned}\frac{d\tilde{x}}{d\tau_{\rm SS}} =& \tilde{f}_{\rm w}^{\beta}\left(\tilde{T}-\tilde{T}_{\rm s}\right)^{\beta-1}\exp\left[\frac{-\beta}{\tilde{T}_{\rm m}}\left(\frac{1}{\tilde{T}}-1\right)\right]\\ &-\tilde{\Pi}\tilde{f}_{\rm w}^{2\beta}\left(\tilde{T}-\tilde{T}_{\rm s}\right)^{2\beta}\exp\left[\frac{-2\beta}{\tilde{T}_{\rm m}}\left(\frac{1}{\tilde{T}}-1\right)\right]\\ &\times\tilde{x}\left(\tilde{T}-\tilde{T}_{\rm sol,dry}+\tilde{\lambda}\tilde{x}^{\gamma}\right)^{\theta}.\end{aligned} \quad (17)$$

In Equation (17), the non-dimensional solidus depression coefficient is $\tilde{\lambda}=\tilde{K}(\omega_0\tilde{f}_{\rm b}/f_{\rm m})^{\gamma}$, the degassing coefficient is $\tilde{\Pi}=\Pi/D$, where

$$\Pi=\rho_{\rm m}d_{\rm melt}f_{\rm degas,\oplus}\frac{\omega_0\tilde{f}_{\rm b}}{f_{\rm m}}\left(\tilde{T}_{\rm liq,dry}-\tilde{T}_{\rm sol,dry}\right)^{-\theta}, \quad (18)$$

and the regassing coefficient (related to the hydrated layer depth) is

$$D=x_{\rm h}\rho_{\rm c}\chi_{\rm r}h^{(1-3\beta)}\frac{(T_{\rm serp}-T_{\rm s})}{T_{\rm ref}^{1+\beta}}\left(\frac{\kappa{\rm Ra}_{\rm crit}\eta_0}{\alpha\rho_{\rm m}gf_{\rm w}(\tilde{x}=1)}\right)^{\beta}, \quad (19)$$

and $\tau_{\rm SS}=tD/\Sigma$, where

$$\Sigma=M\omega_0\tilde{f}_{\rm b}\frac{h^{(1-6\beta)}\kappa^{(2\beta-1)}}{10.76L_{\rm MOR}}\left(\frac{{\rm Ra}_{\rm crit}\eta_0}{\alpha\rho_{\rm m}gT_{\rm ref}f_{\rm w}(\tilde{x}=1)}\right)^{2\beta} \quad (20)$$

is related to the spreading rate. In our coupled integrations of Equations (7) and (17) we ensure that the hydrated layer does not contain more water than the surface in order to maintain water mass balance (Schaefer & Sasselov 2015). This is a key assumption that ensures that the amount of water in the mantle never exceeds the total amount of water in the planet.

2.2.3. *Seafloor pressure-dependent degassing and temperature-dependent regassing*

In this section, we construct a model where the degassing rate is determined by seafloor pressure (as volcanism rates will be lower if overburden pressure is higher) and the regassing rate is determined by the mantle temperature (as the depth of serpentinization will be lower if temperature is higher). We construct such a model because serpentinization can only happen below a critical temperature, whereas it has not been conclusively shown to depend on overburden pressure. Meanwhile, it has been shown that volcanism rates on exoplanets should be inversely related to the overburden pressure (Kite et al. 2009). In this model, the degassing rate is taken from Equation (11) with $\mu=1$ (the value expected from Kite et al. 2009) and the regassing rate from Equation (16). Using the same method as in Sections 2.2.1 and 2.2.2, we substitute these into Equation (9) and nondimensionalize (see Appendix A.3 for more details). Doing so, we find

$$\begin{aligned}\frac{d\tilde{x}}{d\tau_{\rm hyb}} =& \tilde{f}_{\rm w}^{\beta}\left(\tilde{T}-\tilde{T}_{\rm s}\right)^{(\beta-1)}\exp\left[\frac{-\beta}{\tilde{T}_{\rm m}}\left(\frac{1}{\tilde{T}}-1\right)\right]\\ &-\tilde{E}\tilde{f}_{\rm w}^{2\beta}\left(\tilde{T}-\tilde{T}_{\rm s}\right)^{(2\beta)}\exp\left[\frac{-2\beta}{\tilde{T}_{\rm m}}\left(\frac{1}{\tilde{T}}-1\right)\right]\\ &\times\tilde{x}\left[\tilde{g}^2\left(\tilde{\omega}-\tilde{x}\right)\right]^{-1},\end{aligned} \quad (21)$$

where $\tilde{E}=E/D$, $E=\rho_{\rm m}d_{\rm melt}f_{\rm degas,\oplus}\omega_0\tilde{f}_{\rm b}/f_{\rm m}$, and $\tau_{\rm hyb}=\tau_{\rm SS}=tD/\Sigma$.

3. COMPARISON OF VOLATILE CYCLING PARAMETERIZATIONS

3.1. *Time-dependent*

Before turning to the steady-state solutions, we compare directly the time-dependent evolution of the three models. Figure 2 shows such a comparison for Earth-like parameters. Each model reaches a steady state after a time $\tau\approx1$, with a value that is independent of initial conditions (not shown). Figure 2 shows that although the mantle temperature evolution does not vary by more than $\sim15\%$ among models, the evolution and steady-state value of mantle water mass fraction varies greatly. Notably, the degassing parameterizations lead to different values of the steady-state mantle water mass fraction $\tilde{x}$ even though both the hybrid and solely temperature-dependent models have their late volatile evolution determined by water mass balance between the hydrated layer and surface. We will explain this in detail in the steady-state solutions of Section 3.2.

Figure 2 also shows the evolution of the non-dimensional ocean depth for each of the models considered. To determine the ocean depth for a given $\tilde{x}$, we utilize Equation (15) of Cowan & Abbot (2014). This relates ocean depth to seafloor pressure by $\tilde{d_{\rm w}}=P/(g\rho_{\rm w})$, where $d_{\rm w}$ is the ocean depth and $\rho_{\rm w}$ the density of water. Non-dimensionalizing, we find

$$\tilde{d_{\rm w}}=\tilde{g}\left(\tilde{\omega}-\tilde{x}\right), \quad (22)$$

where $\tilde{d_{\rm w}}=d_{\rm w}/d_{\rm w,\oplus}$ is the ocean depth normalized to that of Earth, $d_{\rm w,\oplus}=4$ km. Note that gravity comes into Equation (22) from the ratio of planetary mass to area, which is proportional to gravity. The evolution of ocean depth with time hence has an opposite sign to that for the mantle water mass fraction, with the hybrid model having the deepest oceans and the Schaefer & Sasselov (2015) model the least end-state surface water.

The models in Section 2.2.2 and Section 2.2.3 have an initial phase of degassing from the mantle followed by strong regassing of water back to the mantle. Note that this initial phase of degassing occurs over a shorter timescale than the low-viscosity ("boundary-layer") model of Schaefer & Sasselov (2015), as we assume that all of the water is in melt (thereby increasing the amount able to be outgassed) and use a higher initial mantle temperature. The steady-state then occurs approximately when the mantle temperature drops below the melting temperature, which reduces the efficiency of degassing greatly. In this state, the regassing rate goes to zero because the hydrated layer becomes saturated at a total water mass equal to that on the surface. Such a steady-state was not found in the volatile cycling models of Sandu et al. (2011) and Schaefer & Sasselov (2015), which utilized parameterized convection. This is because the evolution was either too slow[2] to reach steady-state over the age of the observable universe or because slow ingassing continued to deplete the surface water reservoir.

[2] This occurrs in models that consider the viscosity as an average mantle viscosity rather than that relevant for the interface between the boundary layer and mantle interior. We do the latter in this work.

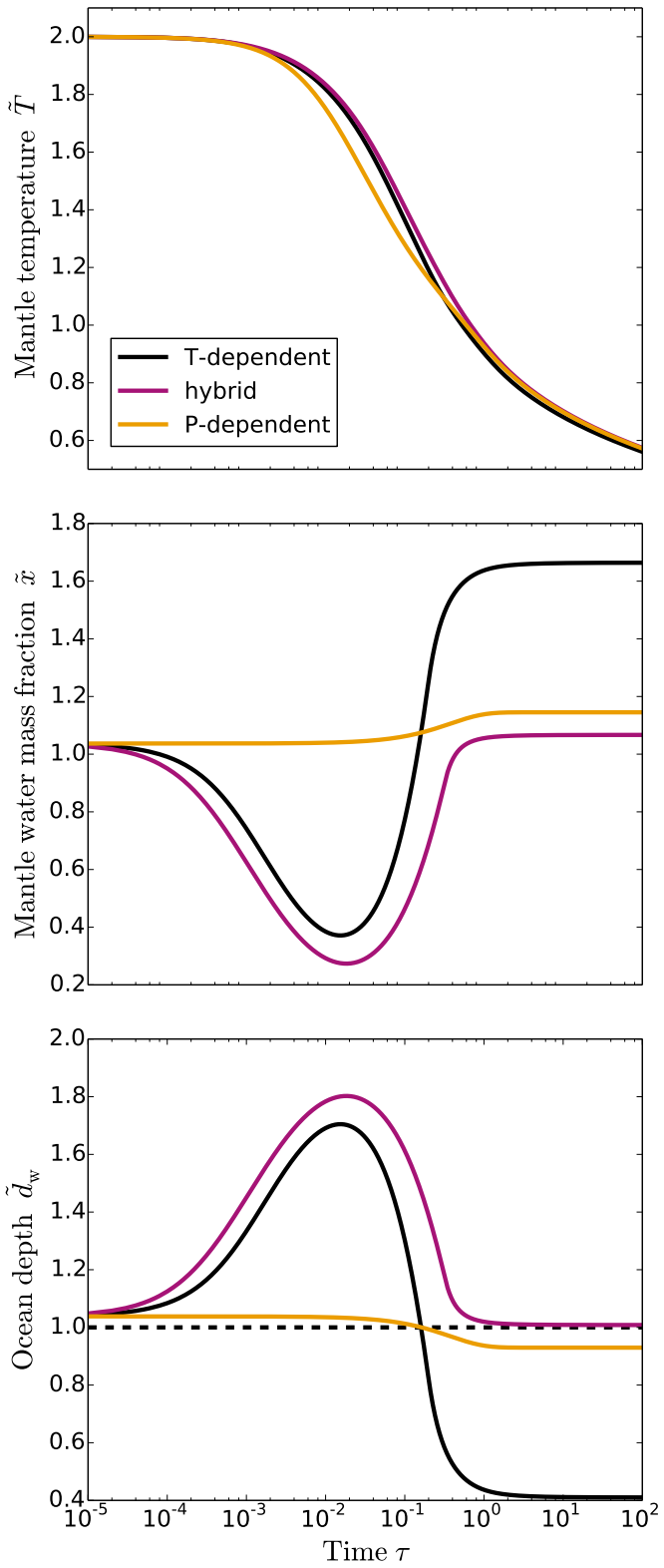

FIG. 2.— Comparison between evolution of temperature, mantle water mass fraction, and ocean depth for models in Sections 2.2.1, 2.2.2, and 2.2.3. Integrations were performed for Earth-like parameter values: $\tilde{M} = 1$, $\tilde{\omega} = 2.07$, $\tilde{x}_0 = \tilde{\omega}/2$, $\tilde{T}_0 = 2$. The dashed line on the ocean depth plot shows the ocean depth of Earth. Note that the ocean depth at which the model would result in a waterworld is $\tilde{d}_w = 2.85$, above the y-axis limit. All models reach an eventual steady-state in mantle water mass fraction, although their mantles perpetually cool. "P-dependent" corresponds to the model in Section 2.2.1, "T-dependent" the model in Section 2.2.2, and "hybrid" the model in Section 2.2.3.

As discussed in Section 1.2, Earth is likely currently at or near a steady-state in surface water mass fraction. We can estimate the steady-state ocean depths for our models as a function of planetary parameters, and will do so in Section 3.2.

We can qualitatively understand the varied evolution in different models by examining how the degassing and regassing rates vary with temperature and/or pressure. Note that the initial phase of degassing from the mantle occurs whether the degassing is temperature or seafloor pressure-dependent, as long as regassing of water back into the mantle is temperature-dependent. This is because initially the regassing rate is very low due to the smaller hydrated layer thickness when the mantle is hot. Regassing then becomes more efficient as the mantle temperature drops and the hydrated layer thickness grows. Similarly, degassing becomes less efficient at later times. This because the mantle is cooler and hence has a lower melt fraction and the seafloor pressure is greater, both decreasing the rate of volcanism.

Because of the increasing regassing and decreasing degassing rates at late times, all of our models reach a steady-state in water abundance. The Schaefer & Sasselov (2015) model has the lowest steady-state surface water mass fraction, as at late times the degassing rate becomes small due to the lack of melt when the mantle temperature is below the solidus. The Cowan & Abbot (2014) and hybrid models have higher steady-state surface water reservoirs because their degassing rate is not related to the mantle temperature and hence is larger at late times. Next, we explore steady-state solutions in order to make predictions of the waterworld boundary for each volatile cycling model.

3.2. *Steady-state mantle water mass fraction*

Given that all of our models reach a steady-state in water partitioning on the timescale of a few billion years, we examine steady-state solutions to the models in Sections 2.2.1-2.2.3. We do so because these steady-states are the most observationally relevant, as most planets in the habitable zone will lie around $\sim$ Gyr-age main-sequence stars. We note that steady-state occurs at $\tilde{T} \leq \tilde{T}_{\rm sol,dry}$ for the model adapted from Schaefer & Sasselov (2015) (from Section 2.2.2). This is because below this temperature, degassing is unimportant. As a result, we calculate the steady-state using $\tilde{T} = \tilde{T}_{\rm sol,dry}$. Solving for the steady-state of Equations (12), (17), and (21) gives

$$\tilde{x} = \tilde{X}_{\oplus} \left[\tilde{g}^2(\tilde{\omega} - \tilde{x})\right]^{\mu+\sigma} \tag{23}$$

for the Cowan & Abbot (2014) model in Section 2.2.1,

$$\tilde{x} = \tilde{\Pi}^{-1} \tilde{f}_{\rm w}^{-\beta} \left(\tilde{T} - \tilde{T}_{\rm s}\right)^{-(1+\beta)} \exp\left[\frac{\beta}{\tilde{T}_{\rm m}}\left(\frac{1}{\tilde{T}} - 1\right)\right] \left(\tilde{\lambda}\tilde{x}^{\gamma}\right)^{-\theta} \tag{24}$$

for the Schaefer & Sasselov (2015) model in Section 2.2.2, and

$$\tilde{x} = \tilde{\omega}\left(1 + \tilde{E}\tilde{f}_{\rm w}^{\beta}\left(\tilde{T} - \tilde{T}_{\rm s}\right)^{1+\beta} \exp\left[\frac{-\beta}{\tilde{T}_{\rm m}}\left(\frac{1}{\tilde{T}} - 1\right)\right] \tilde{g}^{-2}\right)^{-1} \tag{25}$$

for the hybrid model in Section 2.2.3. Equation (23) reproduces Equation (20) of Cowan & Abbot (2014). Note

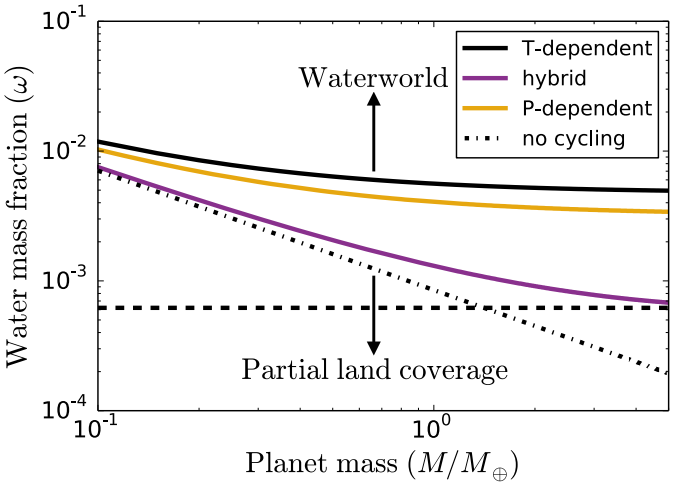

FIG. 3.— Waterworld boundary as a function of total water mass fraction and planet mass (normalized to that of Earth) for the volatile cycling models considered. All fixed parameters are at their fiducial values (Table 1). Planets above each line are waterworlds, and planets below the line have partial land coverage. The dashed line shows the approximate value of Earth's total water mass fraction assuming that the mantle has 2.5 Earth ocean masses of water (Cowan & Abbot 2014). The dot-dashed line shows what the waterworld boundary would be if water cycling did not occur and all of the planetary water resided on the surface. The model of Cowan & Abbot (2014) predicts that planets require a much larger total mass of water to become waterworlds than the hybrid model, but has a similar waterworld boundary to that of Schaefer & Sasselov (2015). The minimum water mass fraction to become a waterworld for the hybrid model decreases strongly with planet mass, meaning that super-Earths are more likely to become waterworlds if degassing is temperature-independent but regassing temperature-dependent.

that the steady-state value of $\tilde{x}$ for the model in Section 2.2.2 is independent of $\tilde{\omega}$. This greatly limits the relative amount of water that can be put into the mantle of planets with large total water fractions.

Equations (23)-(25) give us transcendental expressions for the steady-state mantle water mass fraction as a function of mantle temperature and planet mass for each model. In Section 4 we solve Equations (23)-(25) and relate the mantle water mass fraction to the surface ocean depth to determine the waterworld limit for various assumptions about the processes that control volatile cycling on exoplanets.

4. WHAT DETERMINES IF A PLANET WILL BE A WATERWORLD?

In this section, we use our steady-state solutions from Section 3.2 to make predictions of the minimum total water mass fraction needed to become a waterworld for a given planet mass. As in Cowan & Abbot (2014), in this calculation we keep $\tilde{x}$ below its petrological limit of (0.7% by mass) or 12 ocean masses for an Earth-mass planet with a perovskite mantle. In our notation, this means $\tilde{x}_{\max} = 15.9$. The mantles of super-Earths will be largely post-perovskite (Valencia et al. 2007b), which may hold more water than perovskite, up to $\approx 2\%$ by mass (Townsend et al. 2015). We do not include such a phase transition in our model, but note that an increase in the maximum water fraction linearly translates to an increase in the total water fraction at which a planet becomes a waterworld. This will be explored further in the sensitivity analysis of Section 5.1.

To determine whether a planet is a waterworld, we compare the steady-state ocean depth calculated from Equation (22) to the maximum depth of water-filled ocean basins (Equation 11 of Cowan & Abbot 2014)

$$\tilde{d}_{\rm o,max} \approx \frac{d_{\rm o,max,\oplus}}{d_{\rm w,\oplus}} \tilde{g}^{-1}, \tag{26}$$

where $\tilde{d}_{\rm o,max,\oplus} = 11.4$ km. If $\tilde{d}_{\rm w} > \tilde{d}_{\rm o,max}$, the planet is a waterworld.

Figure 3 shows the waterworld boundary as a function of total water mass fraction and planet mass for all three volatile cycling models considered here. As shown in Cowan & Abbot (2014), mantle temperature-independent volatile cycling models predict that a large water mass fraction ($0.3 - 1\%$) is needed for a planet to become a waterworld, with only a slight dependence on planet mass. The model of Schaefer & Sasselov (2015) predicts a similar but slightly larger water fraction than that of Cowan & Abbot (2014). This is because the mantles in the Schaefer & Sasselov (2015) model are at their petrologic limit of water mass fraction.

The hybrid model, meanwhile, predicts that a much lower total water mass fraction is needed for a planet to become a waterworld. The limiting water mass fraction decreases more strongly with increasing planet mass in this model, meaning that super-Earths are more likely to be waterworlds if the hybrid model is physically relevant. However, this limiting water mass fraction remains larger than in the case without volatile cycling (dot-dashed line in Figure 3). Notably, the waterworld boundary reaches Earth's water mass fraction for $\approx 5 M_\oplus$ planets. This is because the hybrid model does not have temperature-dependent degassing, and therefore degassing does not decrease strongly in efficacy at late times when the mantle is cool. Instead, degassing of water at mid-ocean ridges reaches a true steady state with the temperature-dependent regassing when the surface ocean becomes deep enough to slow down the degassing rate. This is unlike the Schaefer & Sasselov (2015) model, in which a steady-state is only reached because there is a limit to the rate and amount of total regassing. Instead, it is more similar to weakening the pressure-dependence of the Cowan & Abbot (2014) model from power-law exponents $\sigma + \mu = 2$ (their nominal model) to $\sigma + \mu = 1$, as the hybrid model effectively sets their degassing exponent $\mu = 1$ and regassing exponent $\sigma = 0$. As we discuss in Section 5.4, the stark differences between the waterworld water-mass limit in the hybrid model and the Cowan & Abbot (2014) and Schaefer & Sasselov (2015) may be potentially observable.

5. DISCUSSION

5.1. *Sensitivity Analysis*

In this section, we perform a sensitivity analysis to determine how the non-dimensional parameters affect our steady-state solutions from Section 3.2. The key unknown parameters that affect our solutions are the maximum mantle water mass fraction $\tilde{x}_{\max}$ (which affects all models), Earth mantle water mass fraction $\tilde{X}_\oplus$ and seafloor pressure power-law exponents $\mu+\sigma$ for the model of Cowan & Abbot (2014), degassing coefficient $\tilde{\Pi}$ for the Schaefer & Sasselov (2015) model, degassing coefficient $\tilde{E}$ in the hybrid model, and surface temperature $\tilde{T}_{\rm s}$ for both

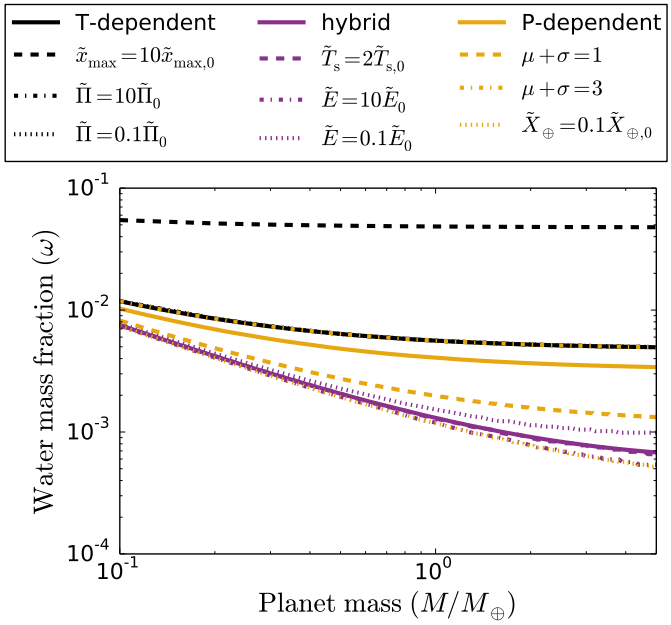

FIG. 4.— Analysis of the sensitivity of the waterworld boundary to varying non-dimensional parameters. The solid lines reproduce the waterworld boundary from Figure 3, while dashed, dashed-dotted, and dotted lines with a given color show the changes in the wateworld boundary for the corresponding model. For the Schaefer & Sasselov (2015) model, increasing the maximum value of mantle water mass fraction correspondingly moves the waterworld boundary up in total water mass fraction. Varying $\tilde{\Pi}$ has no effect because the model has already increased the mantle water mass fraction to its maximal value. For the Cowan & Abbot (2014) model, decreasing $\mu+\sigma$ decreases the total water fraction needed to become a waterworld. Increasing $\mu+\sigma$ increases the waterworld boundary, but the mantle reaches its petrological limit of mantle water mass fraction if $\mu+\sigma=3$. Decreasing $\tilde{X}_\oplus$ decreases the waterworld boundary by a similar fraction, and increasing $\tilde{X}_\oplus$ similarly increases the boundary until the maximum water mass fraction is reached (not shown). For the hybrid model, varying surface temperature plays little role in changing the waterworld boundary. Increasing $\tilde{E}$ slightly decreases the water mass fraction to become a waterworld, but this is a relatively small effect. Our conclusion that the total water mass fraction needed to become a waterworld is much smaller for the hybrid model is hence robust to uncertainties in parameter values.

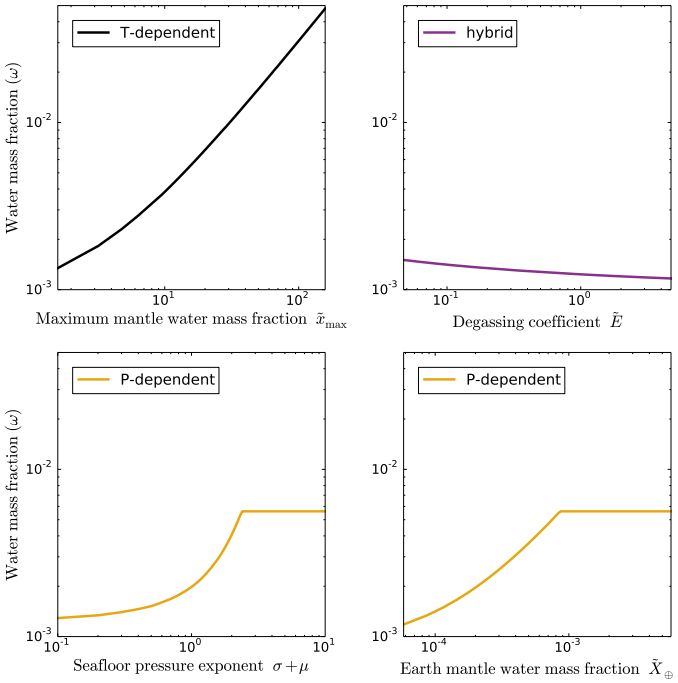

FIG. 5.— Sensitivity analysis on the waterworld boundary for varying non-dimensional parameters with a fixed $M/M_\oplus=1$. We vary the parameters that have the largest impact on the waterworld boundary: $\tilde{x}_{\max}$ for the Schaefer & Sasselov (2015) model, $\tilde{E}$ for the hybrid model, and $\sigma+\mu$ and $\tilde{X}_\oplus$ for the Cowan & Abbot (2014) model. The waterworld boundary for the Schaefer & Sasselov (2015) model is strongly dependent on $\tilde{x}_{\max}$. The boundary for the Cowan & Abbot (2014) model is dependent on $\sigma+\mu$ and $\tilde{X}_\oplus$ up to the limit where the mantle becomes saturated with water. The results of the hybrid model are only marginally sensitive to $\tilde{E}$, giving us confidence that the hybrid model indeed lowers the planetary water mass fraction needed to become a waterworld.

the Schaefer & Sasselov (2015) and hybrid models. Importantly, our steady-states are independent of the abundance of radiogenic elements, eliminating some of the natural variation between planetary systems. Though the abundance of radiogenic elements affects the time it takes to reach steady-state, the steady-state volatile cycling is independent of the decreasing mantle temperature at late times. Figure 4 shows how varying these parameters in each model affects our derived waterworld boundary.

Though the changes in the waterworld boundary with changing $\mu+\sigma$ have been explored in Cowan & Abbot (2014), we reproduce them here for comparison with the other models. Decreasing the dependencies of degassing and regassing on seafloor pressure reduces the water mass fraction at which the surface is completely water-covered, with a maximum decrease of a factor of 2 between the $\mu+\sigma=2$ and $\mu+\sigma=1$ cases. Similarly, increasing the dependence to $\mu+\sigma=3$ increases the limiting water mass fraction to become a waterworld, but the model reaches the maximum mantle water mass fraction. If $\tilde{X}_\oplus$ is a factor of ten lower than used here, the waterworld boundary decreases by a comparably large fraction, especially for super-Earths. If $\tilde{X}_\oplus$ is much larger than assumed here, the mantle will be at its petrological limit of water intake and the waterworld boundary will be determined by the maximum mantle water mass fraction.

For the model of Schaefer & Sasselov (2015), which is at the petrological limit of maximum mantle water mass fraction, varying $\tilde{\Pi}$ by an order of magnitude in either direction does not change the waterworld boundary. However, increasing the maximum mantle water mass fraction by a given value increases the total water mass fraction needed to become a waterworld by a comparable amount.

For both the hybrid model and the Schaefer & Sasselov (2015) model, changing the surface temperature only leads to minute changes in the waterworld boundary. This is because the surface temperature cannot vary by more than a factor of a few or else liquid water would not be stable on the surface. Increasing $\tilde{E}$ in the hybrid model decreases the total mass fraction needed to become a waterworld, but by less than a factor of two for all masses.

From Figure 4, we can identify four key non-dimensional parameters that change the waterworld boundary by a sizeable amount: $\tilde{x}_{\max}$ (which mainly affects the Schaefer & Sasselov 2015 model), $\tilde{E}$ for the hy-

brid model, and $\sigma + \mu$ and $\tilde{X}_\oplus$ for the Cowan & Abbot (2014) model. Figure 5 shows how continuously varying these parameters by one order of magnitude around their fiducial value with a planet mass fixed equal to that of Earth affects the water mass fraction at which planets become waterworlds. As mentioned above, our results are very sensitive to the petrological limit of the mantle water mass fraction, but an order of magnitude increase in $\tilde{E}$, $\sigma + \mu$, and $\tilde{X}_\oplus$ leads to only a factor of ~ 2 or less increase in the waterworld limit. Note that increasing both $\sigma + \mu$ and $\tilde{X}_\oplus$ cannot lead to continuous increases in the waterworld limit, as the petrological limit of water mantle mass fraction is reached just above our fiducial values for these parameters. As a result, the Cowan & Abbot (2014) model is, like the Schaefer & Sasselov (2015) model, sensitive to the maximum mantle water mass fraction $\tilde{x}_{\max}$. Our results are much less sensitive to $\tilde{E}$, for which an order-of-magnitude increase only decreases the waterworld boundary by $\sim 10\%$. As a result, the conclusion that super-Earths are more likely to be waterworlds if degassing is temperature-independent is robust to order-of-magnitude uncertainties in our non-dimensional parameters.

5.2. *Comparison with previous work*

In this work, we developed simplified models for water cycling between the mantle and the surface based on previous models in the literature. We did so in order to compare their predictions for whether or not terrestrial exoplanets will be waterworlds. This is the first such test of physical assumptions that has been performed for volatile cycling on planets with varying mass, though Sandu et al. (2011) explored how models of varying complexity affect volatile cycling on Earth. Our models find that the surface water mass fraction reaches a steady-state after ~ 2 Gyr of evolution. Though this has been found when keeping the ratio of the degassing and regassing rates fixed in time (McGovern & Schubert 1989), no steady-state has previously been found when these rates are dependent on the mantle temperature and allowed to separately evolve.

We find a steady-state in our models for two reasons: the degassing rate is initially larger than the regassing rate (leading to convergent evolution of the two rates), and the volatile evolution is relatively quick. In our temperature-dependent and hybrid models, the volatile evolution is quick because we use a viscosity relevant for the upper mantle, leading to faster evolution than for a viscosity relevant in the deep mantle (Schaefer & Sasselov 2015). Additionally, the regassing rate is limited because the mass of water in the hydrated layer cannot be greater than that on the surface, which as in Schaefer & Sasselov (2015) leads to a sharp decrease in the regassing rate at late times. Given that the degassing rate is also small due to the low temperatures, these rates balance to determine our steady-states and hence waterworld boundary limits from Section 4.

We agree with the conclusion of Cowan & Abbot (2014) that super-Earths are unlikely to be waterworlds for both of the models with solely seafloor pressure-dependent and temperature-dependent water cycling. We also similarly find that conclusion is likely unaffected by parameter uncertainties. However, if these models themselves are less physical than a model with seafloor pressure dependencies dominating the degassing rate and temperature dependencies controlling regassing, that conclusion may change. In this hybrid model, the total mass fraction needed to become a waterworld is much smaller than that in both the Cowan & Abbot (2014) and Schaefer & Sasselov (2015) models. Ideally, future work will help distinguish between the viability of the three models considered here.

5.3. *Limitations*

In this work we considered three separate parameterizations for water cycling between ocean and mantle in order to make predictions for how they might affect exoplanet surface water abundances. We did so because the processes that control volatile cycling on Earth are not understood to the level of detail needed to make predictions for exoplanets with varying masses, total water mass fractions, compositions, and climates. Due to this, we utilized a simplified semi-analytic model and parameterized volatile cycling rates as either a power-law in pressure or a function of temperature. Though this simplified model is powerful for understanding how a given process changes the surface water budget of the suite of exoplanets, studying surface water evolution on a given planet enables the use of more detailed coupling of parameterized convection and volatile cycling as in Sandu et al. (2011); Schaefer & Sasselov (2015).

5.4. *Observational constraints and future work*

It is clear that there is a dichotomy in the waterworld boundary based on whether or not one assumes that volatile cycling is temperature-dependent and/or pressure-dependent. As a result, understanding better which processes control volatile cycling on Earth is important to make more stringent predictions of whether terrestrial exoplanets should be waterworlds. Alternatively, observations with post-*JWST*-era instruments may be able to determine whether or not there is exposed land through either infrared spectra (if the atmosphere is not too optically thick, Abbot et al. 2012) or photometric observations over an entire planetary orbit in many wavelengths (Cowan et al. 2009; Kawahara & Fujii 2010; Cowan & Strait 2013; Cowan & Abbot 2014). This would serve as a test of the different volatile cycling parameterizations. If some super-Earths are found to have non-zero land fraction, the feedback between seafloor pressure and mantle convection is not important or volatile delivery is inefficient for these objects. If, on the other hand, super-Earths are found to all be waterworlds, considering the combined effects of seafloor pressure-limited degassing and mantle convection may be necessary to explain volatile cycling on terrestrial planets.

In the future, one could use sophisticated multi-dimensional calculations of mantle convection including degassing through mid-ocean ridge volcanism and regassing through subduction of hydrated basalt, but this would be computationally expensive. However, these sophisticated calculations will not be worthwhile until the specific processes that govern volatile cycling on Earth and terrestrial exoplanets are understood in detail. We propose, then, that future observations of terrestrial exoplanets will be able to distinguish between the various

water cycling models considered in this work. This will help constrain theories for water cycling on Earth and enable more sophisticated models to make predictions for the surface water inventory of individual planets.

6. CONCLUSIONS

1. Volatile cycling on terrestrial exoplanets with plate tectonics should reach an approximate steady-state on the timescale of a few billion years, independent of the volatile cycling parameterization used. Given that Earth is likely near a steady-state in surface water mass fraction, this gives us confidence that many terrestrial exoplanets around main-sequence stars are also at or near steady-state.

2. Models considering either temperature-dependent degassing and regassing or pressure-dependent degassing and regassing predict that copious amounts of water ($\sim 0.3-1\%$ of total planetary mass) must be present to form a waterworld. These models have their mantles saturated with water, and if the total water mass fraction is high they are at or near the petrological limit for how much water the mantle can hold. The waterworld boundary for the solely temperature-dependent volatile cycling model is determined by this limit. As a result, if a super-Earth mantle can hold more water, the waterworld boundary will move upward by a similar factor. This would make it even less likely for super-Earths to be waterworlds.

3. If seafloor pressure is important for the degassing rate of water but not for regassing, it is more likely that super-Earths will be waterworlds. In this case, a super-Earth with the same total water mass fraction as Earth could become a waterworld. These planets would be less likely to be habitable, as unlucky planets with a large amount of initial water delivery may lack a silicate weathering feedback to stabilize their climates. Understanding further which processes determine volatile cycling on Earth will help us understand what processes control mid-ocean ridge degassing and subduction rates of water on exoplanets with surface oceans.

4. Observations in the future may be able to test which of the volatile cycling models presented here applies to terrestrial exoplanets as a whole. If super-Earths are all found to have some land fraction, then water cycling is determined by temperature-dependent or seafloor pressure-dependent processes alone or volatile delivery rates are low. If super-Earths are instead all found to be waterworlds, either volatile delivery is efficient or the intertwined effects of seafloor pressure-depenent degassing and mantle temperature-dependent regassing determine surface-interior water exchange.

This work was aided greatly by discussions with L. Coogan, N. Cowan, C. Goldblatt, A. Lenardic, L. Schaefer, and K. Zahnle. We thank the Kavli Summer Program in Astrophysics for the setting to perform this research and the hospitality of the program members and community at the University of California, Santa Cruz. TDK acknowledges support from NASA headquarters under the NASA Earth and Space Science Fellowship Program Grant PLANET14F-0038. DSA acknowledges support from the NASA Astrobiology Institute Virtual Planetary Laboratory, which is supported by NASA under cooperative agreement NNH05ZDA001C.

APPENDIX

A. VOLATILE CYCLING SCHEMES: DERIVATION

A.1. *Seafloor-pressure dependent degassing and regassing*

In this section, we write down a time-dependent version of the model from Cowan & Abbot (2014), where degassing and regassing are regulated by seafloor pressure. The regassing and degassing rates in this case are

$$w_{\downarrow} = x_{\rm h}\rho_{\rm c}d_{\rm h}(P)\chi, \tag{A1}$$

$$w_{\uparrow} = x\rho_{\rm m}d_{\rm melt}f_{\rm degas}(P), \tag{A2}$$

equivalent to Equations (10) and (11). Here $x_{\rm h}$ is the mass fraction of water in the hydrated crust, $\rho_{\rm c}$ the density of the oceanic crust, χ the subduction efficiency, $\rho_{\rm m}$ the density of the upper mantle, $d_{\rm melt}$ the depth of melting below mid-ocean ridges, $d_{\rm h}$ the hydrated layer depth and $f_{\rm degas}$ the degassing efficiency. To derive Equation (12), we start with Equation (9) and substitute Equations (A1) and (A2)

$$\frac{dx}{dt} = \frac{L_{\rm MOR}S}{f_{\rm M}M}\left[x_{\rm h}\rho_{\rm c}\chi d_{\rm h,\oplus}\left(\frac{P}{P_\oplus}\right)^{\sigma} - x\rho_{\rm m}d_{\rm melt}f_{\rm degas,\oplus}\left(\frac{P}{P_\oplus}\right)^{-\mu}\right], \tag{A3}$$

where $L_{\rm MOR} = 3\pi R_{\rm p}$ is the mid-ocean ridge length, S is the average spreading rate of Earth (≈ 10 cm year^{-1}), and we have used the power laws

$$d_{\rm h}(P) = d_{\rm h,\oplus}\left(\frac{P}{P_\oplus}\right)^{\sigma}, \tag{A4}$$

$$f_{\rm degas}(P) = f_{\rm degas,\oplus}\left(\frac{P}{P_\oplus}\right)^{-\mu}. \tag{A5}$$

Cowan & Abbot (2014) chose power-laws to illustrate how different strengths of seafloor pressure-dependence would operate. In Equation (A4) $d_{\mathrm{h},\oplus}$ is the hydration depth on Earth, $P_\oplus$ is Earth's seafloor pressure, and in Equation (A5) $f_{\mathrm{degas},\oplus}$ is the melt degassing fraction on modern Earth. Note that seafloor pressure $P = g\rho_{\mathrm{w}} d_{\mathrm{w}}$, where d_{w} is the ocean depth and ρ_{w} the density of water.

Cowan & Abbot (2014) relate seafloor pressure to mantle water mass fraction by

$$P = P_\oplus \tilde{g}^2 \frac{(\omega - x f_{\mathrm{M}})}{\omega_0 \tilde{f}_{\mathrm{b}}}, \tag{A6}$$

where $\omega_0 = 2.3 \times 10^{-4}$ is the fractional mass of Earth's surface water and $\tilde{f}_{\mathrm{b}} = f_b / f_{b,\oplus} = 1.3$ is the ocean basin covering fraction normalized to that of Earth. Plugging this expression for P into Equation (A3), we find

$$\frac{dx}{dt} = \frac{L_{\mathrm{MOR}} S}{f_{\mathrm{M}} M}\left[x_{\mathrm{h}}\rho_{\mathrm{c}}\chi d_{\mathrm{h},\oplus}\left(\tilde{g}^2\frac{(\omega - x f_{\mathrm{M}})}{\omega_0\tilde{f}_{\mathrm{b}}}\right)^{\sigma} - \rho_{\mathrm{m}} d_{\mathrm{melt}} x f_{\mathrm{degas},\oplus}\left(\tilde{g}^2\frac{(\omega - x f_{\mathrm{M}})}{\omega_0\tilde{f}_{\mathrm{b}}}\right)^{-\mu}\right]. \tag{A7}$$

Note that we can write Equation (A7) using $\tilde{\omega} = \omega/(\omega_0\tilde{f}_{\mathrm{b}})$ and $\tilde{x} = x f_{\mathrm{m}}/(\omega_0\tilde{f}_{\mathrm{b}})$ as

$$\frac{dx}{dt} = \frac{L_{\mathrm{MOR}} S}{f_{\mathrm{M}} M}\left[x_{\mathrm{h}}\rho_{\mathrm{c}}\chi d_{\mathrm{h},\oplus}\left[\tilde{g}^2(\tilde{\omega} - \tilde{x})\right]^{\sigma} - \rho_{\mathrm{m}} d_{\mathrm{melt}} x f_{\mathrm{degas},\oplus}\left[\tilde{g}^2(\tilde{\omega} - \tilde{x})\right]^{-\mu}\right]. \tag{A8}$$

Non-dimensionalization of Equation (A8) then gives

$$\frac{d\tilde{x}}{d\tau} = \left[\tilde{g}^2\left(\tilde{\omega} - \tilde{x}\right)\right]^{\sigma} - \tilde{X}_\oplus^{-1}\tilde{x}\left[\tilde{g}^2\left(\tilde{\omega} - \tilde{x}\right)\right]^{-\mu}, \tag{A9}$$

equivalent to Equation (12). In Equation (A9),

$$\tilde{X}_\oplus = \frac{x_h\rho_{\mathrm{c}}\chi d_{\mathrm{h},\oplus} f_{\mathrm{M}}}{\rho_{\mathrm{m}} d_{\mathrm{melt}} f_{\mathrm{degas},\oplus}\omega_0\tilde{f}_{\mathrm{b}}} \tag{A10}$$

is the non-dimensionalized mantle water mass fraction of Earth, $\tilde{\omega} = \omega/(\omega_0\tilde{f}_{\mathrm{b}})$ is the non-dimensionalized total water mass fraction, $\tilde{g} = g/g_\oplus$, and

$$\tau_{\mathrm{CA}} = \tau = t\frac{L_{\mathrm{MOR}} S x_{\mathrm{h}}\rho_{\mathrm{c}}\chi d_{\mathrm{h},\oplus}}{M\omega_0\tilde{f}_{\mathrm{b}}} \tag{A11}$$

is the non-dimensional time, which is inversely related to the seafloor overturning timescale $A/(L_{\mathrm{MOR}}S)$.

A.2. *Temperature-dependent degassing and regassing*

In this section, we derive a simplified version of the Schaefer & Sasselov (2015) model, where volatile cycling rates are determined by the mantle temperature. The regassing and degassing rates in this case are

$$w_\downarrow = x_{\mathrm{h}}\rho_{\mathrm{c}}\chi d_{\mathrm{h}}(T), \tag{A12}$$

$$w_\uparrow = \rho_{\mathrm{m}} d_{\mathrm{melt}} f_{\mathrm{degas},\oplus} f_{\mathrm{melt}}(T) x, \tag{A13}$$

equivalent to Equations (15) and (16). Here we have written the hydrated layer depth as a function of temperature. We have written f_{degas} as $f_{\mathrm{degas},\oplus} f_{\mathrm{melt}}(T)$ where $f_{\mathrm{melt}}(T)$ is the temperature-dependent melt fraction. Inserting Equations (A12) and (A13) into Equation (9), the dimensionful time-derivative of mantle water mass fraction is

$$\frac{dx}{dt} = \frac{L_{\mathrm{MOR}} S(T)}{f_{\mathrm{m}} M}\left[x_{\mathrm{h}}\rho_{\mathrm{c}}\chi_{\mathrm{r}} d_{\mathrm{h}}(T) - \rho_{\mathrm{m}} d_{\mathrm{melt}} f_{\mathrm{degas},\oplus} f_{\mathrm{melt}}(T) x\right]. \tag{A14}$$

The functional forms of $S, d_{\mathrm{h}}, f_{\mathrm{melt}}$ are developed in Section 2.3 of Schaefer & Sasselov (2015). Here we simplify them in order to obtain an analytically tractable version of Equation (A14). Firstly, the spreading rate is defined as

$$S = 2u_{\mathrm{conv}} = 2\frac{5.38\kappa h}{\delta^2}, \tag{A15}$$

The boundary-layer thickness δ is

$$\delta = h\left(\frac{\mathrm{Ra}_{\mathrm{crit}}}{\mathrm{Ra}}\right)^{\beta}. \tag{A16}$$

Substituting δ from Equation (A16),

$$S = \frac{10.76\kappa}{h}\left(\frac{\mathrm{Ra}}{\mathrm{Ra}_{\mathrm{crit}}}\right)^{(2\beta)} = 10.76\kappa^{(1-2\beta)}h^{(6\beta-1)}\left(\frac{\alpha\rho_{\mathrm{m}} g(T - T_{\mathrm{s}})}{\eta(T,x)\mathrm{Ra}_{\mathrm{crit}}}\right)^{2\beta}. \tag{A17}$$

The hydration depth (depth to which rock can be serpentinized) is defined as

$$d_{\rm h} = k\frac{(T_{\rm serp} - T_{\rm s})}{F_{\rm m}}. \tag{A18}$$

Using the mantle heat flux from Equation (1), we find

$$d_{\rm h} = h\frac{(T_{\rm serp} - T_{\rm s})}{(T - T_{\rm s})}\left(\frac{{\rm Ra}_{\rm crit}}{{\rm Ra}}\right)^{\beta} = h^{(1-3\beta)}(T - T_{\rm s})^{-(1+\beta)}(T_{\rm serp} - T_{\rm s})\left(\frac{\eta(T,x)\kappa{\rm Ra}_{\rm crit}}{\alpha\rho_{\rm m}g}\right)^{\beta}. \tag{A19}$$

Lastly, we use the same expression for the melt fraction as Schaefer & Sasselov (2015), which relates the melt fraction to mantle temperature through a power-law, taking into account the solidus depression of wet mantle

$$f_{\rm melt} = \left(\frac{T - T_{\rm sol,wet}(x)}{T_{\rm liq,dry} - T_{\rm sol,dry}}\right)^{\theta}. \tag{A20}$$

Here, we take $T_{\rm liq,dry} \approx 1498$ K, $T_{\rm sol,dry} \approx 1248$ K as constants, and $T_{\rm sol,wet} = T_{\rm sol,dry} - Kx^{\gamma}$, assuming that the mass fraction of water in melt is the same as the mass fraction of water in the mantle. We assume so because the partitioning coefficient of water in the mantle is thought to be extremely small ($\approx 1\%$). Plugging in Equations (A17, A19, A20) into Equation (A14) and non-dimensionalizing gives

$$\begin{aligned}\frac{d\tilde{x}}{d\tau_{\rm SS}} =& \tilde{f}_{\rm w}^{\beta}\left(\tilde{T} - \tilde{T}_{\rm s}\right)^{\beta-1}\exp\left[\frac{-\beta}{\tilde{T}_{\rm m}}\left(\frac{1}{\tilde{T}} - 1\right)\right] \\ &- \tilde{\Pi}\tilde{f}_{\rm w}^{2\beta}\left(\tilde{T} - \tilde{T}_{\rm s}\right)^{2\beta}\exp\left[\frac{-2\beta}{\tilde{T}_{\rm m}}\left(\frac{1}{\tilde{T}} - 1\right)\right]\tilde{x}\left(\tilde{T} - \tilde{T}_{\rm sol,dry} + \tilde{\lambda}\tilde{x}^{\gamma}\right)^{\theta},\end{aligned} \tag{A21}$$

equivalent to Equation (17). Here the non-dimensional solidus depression coefficient is $\tilde{\lambda} = \tilde{K}(\omega_0\tilde{f}_{\rm b}/f_{\rm m})^{\gamma}$ and the degassing coefficient is $\tilde{\Pi} = \Pi/D$, where

$$\Pi = \rho_{\rm m}d_{\rm melt}f_{{\rm degas},\oplus}\frac{\omega_0\tilde{f}_{\rm b}}{f_{\rm m}}\left(\tilde{T}_{\rm liq,dry} - \tilde{T}_{\rm sol,dry}\right)^{-\theta}. \tag{A22}$$

The regassing coefficient (related to the hydrated layer depth) is

$$D = x_{\rm h}\rho_{\rm c}\chi_{\rm r}h^{(1-3\beta)}\frac{(T_{\rm serp} - T_{\rm s})}{T_{\rm ref}^{1+\beta}}\left(\frac{\kappa{\rm Ra}_{\rm crit}\eta_0}{\alpha\rho_{\rm m}gf_{\rm w}(\tilde{x}=1)}\right)^{\beta}, \tag{A23}$$

and $\tau_{\rm SS} = tD/\Sigma$, where

$$\Sigma = M\omega_0\tilde{f}_{\rm b}\frac{h^{(1-6\beta)}\kappa^{(2\beta-1)}}{10.76L_{\rm MOR}}\left(\frac{{\rm Ra}_{\rm crit}\eta_0}{\alpha\rho_{\rm m}gT_{\rm ref}f_{\rm w}(\tilde{x}=1)}\right)^{2\beta}. \tag{A24}$$

To ensure water mass balance in their time-dependent solutions, Schaefer & Sasselov (2015) force the hydrated layer to hold no more water than the surface itself. Formally, this ensures that

$$x_h\rho_{\rm m}\frac{4\pi}{3}\left(R^3 - (R - d_{\rm h})^3\right) \leq M\omega_0\tilde{f}_{\rm b}\left(\tilde{\omega} - \tilde{x}\right). \tag{A25}$$

Noting that we can re-write the hydrated layer depth from Equation (A19) as

$$d_{\rm h} = D_2{\rm exp}\left[\frac{\beta}{\tilde{T}_{\rm m}}\left(\frac{1}{\tilde{T}} - 1\right)\right]\tilde{f}_{\rm w}^{-\beta}\left(\tilde{T} - \tilde{T}_{\rm s}\right)^{-(1+\beta)}, \tag{A26}$$

where $D_2 = D/(x_h\rho_{\rm c}\chi_{\rm r})$, we find a constraint for D_2 to ensure that the hydrated layer water mass is less than or equal to that on the surface:

$$D_2 \leq \left[R - \left(R^3 - \frac{3\omega_0\tilde{f}_{\rm b}M(\tilde{\omega} - \tilde{x})}{4\pi x_{\rm h}\rho_{\rm m}}\right)^{1/3}\right]\exp\left[\frac{-\beta}{\tilde{T}_{\rm m}}\left(\frac{1}{\tilde{T}} - 1\right)\right]\tilde{f}_{\rm w}^{\beta}\left(\tilde{T} - \tilde{T}_{\rm s}\right)^{(1+\beta)}. \tag{A27}$$

We force the constraint from Equation (A27) in each timestep to ensure stability[3]. Using the maximum value of D_2, we can the maximum value of $\tilde{\Pi}$ for use in Equation (17)

$$\tilde{\Pi}_{\rm max} = \frac{\Pi}{D_{2,\rm max}x_h\rho_{\rm c}\chi_{\rm r}}. \tag{A28}$$

[3] If this constraint is not placed, the mantle water mass fraction will go to infinity.

A.3. *Seafloor pressure-dependent degassing and temperature-dependent regassing*

Given the above models with either temperature or seafloor pressure-dependent volatile cycling rates, one can envision a model where surface water abundance is regulated by both seafloor pressure and mantle temperature. Here we consider a hybrid model where seafloor pressure regulates the degassing rate (as volcanism is less efficient with greater overburden pressure) and mantle temperature regulates the regassing rate (because serpentinization cannot occur if temperatures are too high). This hybrid model follows similarly from our derivations in Appendix A.1 and Appendix A.2. The regassing and degassing rates in this case are

$$w_{\downarrow} = x_{\rm h}\rho_{\rm c}\chi d_{\rm h}(T), \tag{A29}$$

$$w_{\uparrow} = x\rho_{\rm m}d_{\rm melt}f_{\rm degas}(P), \tag{A30}$$

equivalent to Equations (A1) and (A13). Inserting these into Equation (9), we find the dimensional form of the time-derivative of water mass fraction

$$\frac{dx}{dt} = \frac{S(T)}{f_{\rm m}M}\left[x_{\rm h}\rho_{\rm c}\chi_{\rm r}d_{\rm h}(T) - \rho_{\rm m}d_{\rm melt}xf_{\rm degas}(P)\right]. \tag{A31}$$

We insert our prescriptions for S and $d_{\rm h}$ from Equations (A17) and (A19), respectively, and the seafloor pressure-dependence of $f_{\rm degas}$ from Equation (A5) into Equation (A31). Non-dimensionalizing, we find

$$\frac{d\tilde{x}}{d\tau_{\rm hyb}} = \tilde{f}_{\rm w}^{\beta}\left(\tilde{T}-\tilde{T}_{\rm s}\right)^{(\beta-1)}\exp\left[\frac{-\beta}{\tilde{T}_{\rm m}}\left(\frac{1}{\tilde{T}}-1\right)\right] - \tilde{E}\tilde{f}_{\rm w}^{2\beta}\left(\tilde{T}-\tilde{T}_{\rm s}\right)^{(2\beta)}\exp\left[\frac{-2\beta}{\tilde{T}_{\rm m}}\left(\frac{1}{\tilde{T}}-1\right)\right]\tilde{x}\left[\tilde{g}^2\left(\tilde{\omega}-\tilde{x}\right)\right]^{-1}, \tag{A32}$$

equivalent to Equation (21). Here $\tilde{E} = E/D$, $E = \rho_{\rm m}d_{\rm melt}f_{\rm degas,\oplus}\omega_0\tilde{f}_{\rm b}/f_{\rm m}$, and $\tau_{\rm hyb} = \tau_{\rm SS} = tD/\Sigma$.

As in to the solely temperature-dependent model, we restrict the hydrated layer depth using Equation (A27). If $D_2 = D_{2,\rm max}$ the corresponding constraint on $\tilde{E}$ is

$$\tilde{E}_{\rm max} = \frac{E}{D_{2,\rm max}x_h\rho_{\rm c}\chi_{\rm r}}. \tag{A33}$$

REFERENCES

Abbot, D. S., Cowan, N. B., & Ciesla, F. J. 2012, The Astrophysical Journal, 756, 178

Cowan, N. B. 2015, arXiv:1511.04444

Cowan, N. B. & Abbot, D. S. 2014, The Astrophysical Journal, 781, 27

Cowan, N. B., Agol, E., Meadows, V. S., Robinson, T., Livengood, T. A., Deming, D., Lisse, C. M., A'Hearn, M. F., Wellnitz, D. D., Seager, S., & Charbonneau, D. 2009, The Astrophysical Journal, 700, 915

Cowan, N. B. & Strait, T. E. 2013, The Astrophysical Journal Letters, 765, L17

Crowley, J. W., Gérault, M., & O'Connell, R. J. 2011, Earth and Planetary Science Letters, 310, 380

Dai, L. & Karato, S.-i. 2009, Earth and Planetary Science Letters, 287, 277

Elkins-Tanton, L. T. 2011, Astrophysics and Space Science, 332, 359

Foley, B. J. 2015, The Astrophysical Journal, 812, 36

Fraine, J., Deming, D., Benneke, B., Knutson, H., Madhusudhan, N., Wilkins, A., & Todorov, K. 2014, Nature, 513, 556

Fressin, F., Torres, G., Charbonneau, D., Bryson, S. T., Christiansen, J., Dressing, C. D., Jenkins, J. M., Walkowicz, L. M., & Batalha, N. M. 2013, The Astrophysical Journal, 766, 81

Hauri, E. H., Gaetani, G. A., & Green, T. H. 2006, Earth and Planetary Science Letters, 248, 715

Hirschmann, M. M. 2006, Annual Review of Earth and Planetary Sciences, 34, 629

Hirth, G. & Kohlstedt, D. 2003, Geophysical Monograph Series, 138, 83

Huang, X., Xu, Y., & Karato, S.-I. 2005, Nature, 434, 746

Inoue, T., Wada, T., Sasaki, R., & Yurimoto, H. 2010, Physics of the Earth and Planetary Interiors, 183, 245

Kasting, J. F. 1988, Icarus, 74, 472

Kasting, J. F. & Holm, N. G. 1992, Earth and Planetary Science Letters, 109, 507

Kasting, J. F., Whitmire, D. P., & Reynolds, R. T. 1993, Icarus, 101, 108

Kawahara, H. & Fujii, Y. 2010, The Astrophysical Journal, 720, 1333

Khan, A. & Shankland, T. J. 2012, Earth and Planetary Science Letters, 317-318, 27

Kite, E. S., Manga, M., & Gaidos, E. 2009, The Astrophysical Journal, 700, 1732

Korenaga, J. 2010, The Astrophysical Journal, 725, L43

Kreidberg, L., Line, M. R., Bean, J. L., Stevenson, K. B., Désert, J.-M., Madhusudhan, N., Fortney, J. J., Barstow, J. K., Henry, G. W., Williamson, M. H., & Showman, A. P. 2015, The Astrophysical Journal, 814, 66

Lenardic, A. & Crowley, J. W. 2012, The Astrophysical Journal, 755, 132

Li, Z. X. A., Lee, C. T. A., Peslier, A. H., Lenardic, A., & Mackwell, S. J. 2008, Journal of Geophysical Research: Solid Earth, 113

Luger, R. & Barnes, R. 2015, Astrobiology, 15, 119

McGovern, P. J. & Schubert, G. 1989, Earth and Planetary Science Letters, 96, 27

Morton, T. D. & Swift, J. 2014, The Astrophysical Journal, 791, 10

O'Neill, C. & Lenardic, A. 2007, Geophysical Research Letters, 34, 2

Pearson, D. G., Brenker, F. E., Nestola, F., McNeill, J., Nasdala, L., Hutchison, M. T., Matveev, S., Mather, K., Silversmit, G., Schmitz, S., Vekemans, B., & Vincze, L. 2014, Nature, 507, 221

Ramirez, R. M. & Kaltenegger, L. 2014, The Astrophysical Journal, 797, L25

Raymond, S., Quinn, T., & Lunine, J. 2004, Icarus, 168, 1

Rowley, D. B. 2013, The Journal of Geology, 121, 445

Sandu, C., Lenardic, A., & McGovern, P. 2011, Journal of Geophysical Research: Solid Earth, 116, 1

Schaefer, L. & Sasselov, D. 2015, The Astrophysical Journal, 801, 40

Schaefer, L., Wordsworth, R., Berta-Thompson, Z., & Sasselov, D. 2016

Sing, D. K., Fortney, J. J., Nikolov, N., Wakeford, H. R., Kataria, T., Evans, T. M., Aigrain, S., Ballester, G. E., Burrows, A. S., Deming, D., Désert, J.-M., Gibson, N. P., Henry, G. W., Huitson, C. M., Knutson, H. A., des Etangs, A. L., Pont, F., Showman, A. P., Vidal-Madjar, A., Williamson, M. H., & Wilson, P. A. 2015, Nature, 529, 18
Sleep, N. 2015, Evolution of the Earth: Plate Tectonics Through Time, Vol. 9 (Elsevier B.V.), 145–172
Tian, F. & Ida, S. 2015, Nature Geoscience Letters, 8, 5
Townsend, J. P., Tsuchiya, J., Bina, C. R., & Jacobsen, S. D. 2015, Physics of the Earth and Planetary Interiors, 244, 42
Turcotte, D. & Schubert, G. 2002, Geodynamics (New York, NY: Cambridge University Press)
Valencia, D. & O'Connell, R. J. 2009, Earth and Planetary Science Letters, 286, 492
Valencia, D., O'Connell, R. J., & Sasselov, D. 2006, Icarus, 181, 545
Valencia, D., O'Connell, R. J., & Sasselov, D. D. 2007a, The Astrophysical Journal, 670, L45
Valencia, D., Sasselov, D. D., O'Connell, R. J., & ;. 2007b, The Astrophysical Journal, 665, 1413
Walker, J. C., Hays, P., & Kasting, J. 1981, Journal of Geophysical Research: Oceans, 86, 9776
Wordsworth, R. D. & Pierrehumbert, R. T. 2013, The Astrophysical Journal, 778, 154